# Estimating the Effect of Higher Order Modes in Spherical Near-Field Probe Correction

Allen Newell, Stuart Gregson

Nearfield Systems Inc.
19730 Magellan Drive,
Torrance, CA 90502-1104

**ABSTRACT**

**The numerical analysis used for efficient processing of spherical near-field data requires that the far-field pattern of the probe can be expressed using only azimuthal modes with indices of μ = ±1.** (1) **If the probe satisfies this symmetry requirement, near-field data is only required for the two angles of probe rotation about its axis of χ = 0 and 90 degrees and numerical integration in χ is not required. This reduces both measurement and computation time and so it is desirable to use probes that will satisfy the μ = ±1 criteria. Circularly symmetric probes can be constructed that reduce the higher order modes to very low levels and for probes like open ended rectangular waveguides (OEWG) the effect of the higher order modes can be reduced by using a measurement radius that reduces the subtended angle of the AUT. Some analysis and simulation have been done to estimate the effect of using a probe with the higher order modes** (2) – (6) **and the following study is another effort to develop guidelines for the properties of the probe and the measurement radius that will reduce the effect of higher order modes to minimal levels. This study is based on the observation that since the higher order probe azimuthal modes are directly related to the probe properties for rotation about its axis, the near-field data that should be most sensitive to these modes is a near-field polarization measurement. This measurement is taken with the probe at a fixed (x,y,z) or (θ,φ,r) position and the probe is rotated about its axis by the angle χ. The amplitude and phase received by the probe is measured as a function of the χ rotation angle. A direct measurement using different probes would be desirable, but since the effect of the higher order modes is very small, other measurement errors would likely obscure the desired information. This study uses the plane-wave transmission equation (7) to calculate the received signal for an AUT/probe combination where the probe is at any specified position and orientation in the near-field. The plane wave spectrum for both the AUT and the probe are derived from measured planar or spherical near-field data. The plane wave spectrum for the AUT is the same for all calculations and the receiving spectrum for the probe at each χ orientation is determined from the far-field pattern of the probe after it has been rotated by the angle χ. The far-field pattern of the probe as derived from spherical near-field measurements can be filtered to include or exclude the higher order spherical modes, and the near-field polarization data can therefore be calculated to show the sensitivity to these higher order modes. This approach focuses on the effect of the higher order spherical modes and completely excludes the effect of measurement errors. The results of these calculations for different AUT/probe/measurement radius combinations will be shown.**

**Keywords:** near-field, measurements, near-field probe, spherical, spherical mode analysis.

## 1.0 Introduction

The spherical near-field theory is based on the transmission equation derived by Jensen (8) – (9) and further developed by Wacker (1) where the antenna under test and the probe are described by spherical mode coefficients that are the coefficients of basis functions that are solutions of Maxwell's equations for a spherical coordinate system. In principle, the transmission equation is valid for any arbitrary test antenna and probe combination at any separation distance between the spherical coordinate system origin and the probe that is outside of the minimum sphere that will completely enclose the antenna under test. The transmission equation is,

$$W^a(\chi,\phi,\theta) = \sum_m \sum_n \sum_\mu \left( \sum_{s=1}^{2} P^{s\mu na} \, Q^{smn} \right) e^{im\phi} \, d^{(n)}_{m\mu}(\theta) \, e^{i\mu\chi} \quad (1)$$

Where $W^a$ is the amplitude and phase data measured by the probe at the radius a and the position defined by the spherical coordinates $\theta$ *and* $\phi$. $\chi$ is the rotation angle of the probe about its z-axis. The P's are the spherical mode coefficients for the probe and the Q's are the corresponding spherical mode coefficients for the antenna under test. Mathematical orthogonality is used to solve the transmission equation in order to obtain the coupling

product which is the product within the brackets of equation 1. The result is shown in equation 2.

$$I^{m'\mu'n'a} = \frac{1}{8\pi^2}\int_0^{2\pi}\int_0^{2\pi}\int_0^{2\pi} W^a(\chi,\theta,\phi)\left( e^{-im'\phi}\, d^{(n')}_{m'\mu'}(\theta)\, e^{i\mu'\chi}\right) \times \sin\theta\, d\theta\, d\phi\, d\chi \tag{2}$$

***Where,***

$$I^{m'\mu'n'a} = P^{1\mu'n'a}\, Q^{1m'n'} + P^{2\mu'n'a}\, Q^{2m'n'}$$

In order to perform the integration for the three angular variables $\theta, \phi$ *and* $\chi$ using incrementally measured data, the data point spacing for all three angles must satisfy the sampling criteria for each variables. Theoretical guidelines are available to specify the angular spacing in $\theta$ and $\phi$ in terms of the radius of the minimum sphere that will completely enclose the antenna. Experimental tests on a given test antenna and probe can also be carried out to verify these guidelines by taking closely spaced data and comparing the far field pattern results when the data point spacing is increased. For an arbitrary probe and measurement radius, satisfying the sampling criteria for the $\chi$ variable would require measurements at small increments in $\chi$ and numerical integration of the data in $\chi$. The required multiple measurements over the complete sphere for small increments in $\chi$ would be very time-consuming and the numerical integration could be both time-consuming and inaccurate. To solve this problem, Wacker(1) proposed using a special probe that would have a symmetry in its far field pattern such that the spherical mode coefficients for the probe would be zero for all $\mu$ values except $\mu = \pm 1$. Such probes are referred to as first-order probes. When the probe satisfies this condition, measurements are only required for $\chi = 0$ and 90 deg and numerical integration of the data for the $\chi$ variable is not required. This greatly reduces the measurement time and results in a fast, efficient and accurate numerical technique to perform the calculations defined in equation 2. The vast majority of the software used in processing spherical near-field data uses this numerical technique and the assumption that the probe satisfies the $\mu = \pm 1$ requirement is implicit in using this software. Probes can be constructed which satisfy this requirement to a very high degree by using a circularly symmetric probe aperture and a precise transition from rectangular to circular waveguide. The spherical mode coefficients for $\mu \neq \pm 1$ of carefully constructed probes are typically at least 40 dB below the first order modes. But such special probes increase the cost of the measurement system and the probes may have a smaller bandwidth than similar rectangular open ended waveguide probes (OEWG). It has been established that if the measurement radius is large enough, probes such as the OEWG can be used for spherical near-field measurements and the effect of their higher order modes will be negligible and the efficient data processing algorithms can be used without causing a significant error in the results. There is only limited information on how large the radius must be and what the residual effects of the higher-order modes are. This study was undertaken to try and answer some of those questions using a technique that had not been tried before and that should be a very sensitive test.

## 2.0 Simulation Concept

Ideally it would be desirable to perform a series of spherical near-field measurements using two separate probes having identical far field patterns except for their pattern characteristics for rotation about the z-axes of the probes. One probe would satisfy the first order mode requirements and have non-zero spherical mode coefficients for only $\mu = \pm 1$. The second probe would have the same on-axis axial ratio and tilt angle and the same spherical mode coefficients for the $\mu = \pm 1$ modes. However it would also have non-zero spherical mode coefficients for other $\mu$ values. This type of probe is referred to as a higher-order probe. Complete spherical near-field measurements could be performed for different test antennas and measurement radii using the two different probes and the far field patterns calculated using the same efficient numerical algorithms which use only the $\mu = \pm 1$ probe coefficients. A comparison of the patterns, polarization, gain and other parameters could then be used to quantify the effect of the higher-order probe when using the software that assumes the probe is a first-order probe.

Another conceptual measurement comparison would require fewer measurements and perhaps be a more sensitive test for the effect of differences in the two probes since it focuses on the specific near-field data that should be most sensitive to the probe characteristics described by the $\mu$ coefficients. In this measurement the first-order probe would be placed at a fixed radius and a fixed $\theta$ *and* $\phi$ position on the measurement sphere. The probe would then be rotated about its z-axis in small increments and the received amplitude and phase recorded as a function of the rotation angle $\chi$. This would produce a near-field polarization curve similar to those shown in Figure 14. The same measurement would be repeated with the higher-order probe and the polarization patterns could then be compared and the differences used to estimate the effect that the higher-order probe would have on far-field results. This measurement comparison could then be repeated for other radii and $\theta$ *and* $\phi$ positions and for other test antennas. This measurement should be very sensitive to the $\mu$ mode properties of the probe since it is the probe's property due to rotation about its z-axis that is different, the

measurement involves only a rotation of the probe about its z-axis, and the measured data will have a large dynamic range in both amplitude and phase. While both of these measurements will be affected by measurement errors such as scattering, positioning errors, leakage and random errors, that may in fact be larger than the probe mode affects being tested, the latter technique may be less sensitive to these measurement errors since it is performed at a single position and requires much less measurement time.

An actual measurement of either type is not practical however since it is not possible to construct two different probes that are identical in every respect except their μ-mode coefficients. And since the effect that is being investigated is likely very small for some measurement configurations, any small imperfections in the construction of the probes would lead to erroneous results.

It is possible to simulate the second measurement to a very high precision that will not be affected by measurement errors or imperfections in the construction of the probes. The simulation can also be accomplished using actual test antennas and probe data and accommodate computations for large data arrays within a reasonable amount of time. The steps in the simulation are as follows.

A planar near-field data file is selected for the antenna under test that contains both main and cross-polarized data from a previous measurement. The data is processed using the standard near-to-far field transformation that includes a correction for the effect of the measuring probe. The far electric field pattern is computed producing the Ludwig II AZ and EL (10) vector components on a grid that is equally spaced in $\frac{k_x}{k}$ and $\frac{k_y}{k}$ over the span form -1 to +1 and saved in an output file for further processing. Output files were produced for array sizes of Nx = Ny = 256, 512, 1024 and 2048 and all were used at some stage in the processing. Since the simulation polarization pattern results will not be compared to any actual measured data, this far-field data file is an error-free representation of a hypothetical antenna that is similar to the antenna used in the actual measurement. Measurement errors due to multiple reflections, truncation, scattering, position errors, flexing cables and probe correction are present in the measured data and the far field patterns. But the far-field pattern produced represents a hypothetical antenna, and since the same data will be used for both simulated probes, the measurement errors will have no effect on the comparison that will be calculated other than being for a specific hypothetical antenna. Other data sets can also be used to represent different test antennas and this will be discussed in the following sections.

A previously measured spherical near-field data file is then selected where a rectangular OEWG was the antenna under test and measurements had been performed at the same frequency as the planar measurements. This measured data is processed using the spherical transformation software to produce a far-field pattern where the Ludwig II $\theta$ and $\phi$ vector components are calculated and saved using a spherical coordinate grid in $\theta$ and $\phi$ where $\theta$ varies from 0 to 90° and $\phi$ varies from 0 to 360°. Angular increments from 0.1º to 1° were used so that different pattern resolutions could be tried in the simulation. One set of output files filtered the spherical mode coefficients in the $\theta$ -index n using the MARS (11) – (12) processing to reduce the effect of scattering and produce smoother patterns as a function of $\theta$, but no filtering was applied to the spherical mode coefficients as a function of the m-index which corresponds to the $\mu$ -index when the OEWG is used as a probe in a spherical measurement. These output files then represent an error-free far-field pattern for a hypothetical OEWG probe that includes all of the modes for a higher order probe.

A second set of output files were also produced using the same angular spans and spacings and the same MARS processing and filtering in the $\theta$ -index n as the first set. But for these output files, filtering was also applied to retain only the m = ±1 spherical modes in the calculation of the far-field pattern. These files then represent an error-free far field pattern for a hypothetical probe that is identical to the first probe except for the elimination of the higher-order mode coefficients. Figures 1 and 2 show the spherical mode amplitude plots for s=1 for the two probes.

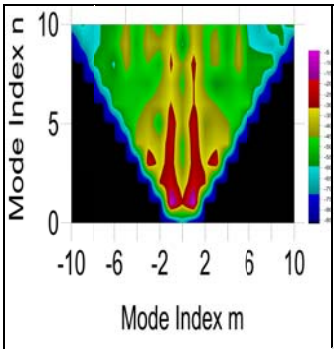


Figure 1-Spherical mode coefficient amplitudes for s=1 for higher-order probe with all m modes retained.

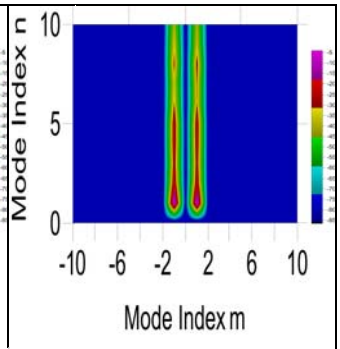


Figure 2-Spherical mode coefficient amplitudes for s=1 for first-order probe with only m = +1, -1 modes.

For the remaining steps in the simulation a computer program was developed to read in the data files for the antenna under test and the probes and produce a near-field polarization measurement at an arbitrary X, Y, and Z position. A polarization results was produced for both of the probes and then compared to determine the effect of

the nonsymmetrical probe. The polarization curve was produced using the planar near-field transmission equation which is shown in equation 3.

$$b_0'(x,y,z,\chi) = F' a_0 \iint \vec{t}_{10}(\vec{K}) \bullet \vec{s}_{02}'(\vec{K},\chi) e^{i\gamma z} e^{i(k_x x + k_y y)} dk_x dk_y$$

***where***

$a_0$ = Input amplitude and phase to AUT

$b_0'(x,y,z,\chi)$ = Probe output amplitude and phase for probe at (x,y,z) and rotated about the probe z-axis by the angle $\chi$

$\vec{t}_{10}(\vec{K})$ = AUT plane-wave transmitting spectrum

$\vec{s}_{02}'(\vec{K},\chi)$ = Probe plane-wave receiving spectrum for $\chi$ rotation

(3)

The rotation angle $\chi$ has been added as a variable to the probe output and the probe receiving spectrum to show that the transmission equation will be used to produce polarization data by evaluating the equation using a series of rotated probe patterns. The planar transmission equation can be used for the simulation as well as the spherical transmission equation since both are equally valid and accurate expressions for the transmission between a test antenna and a probe at any arbitrary near-field position and relative orientation. The planar equation is much easier to calculate numerically and can be used without modification for both first-order and higher-order probes.

The steps in the computer program will be described and illustrated for a specific example. The probe pattern data file for the higher-order probe using spacing in $\theta$ of 0.2° and a $\phi$ spacing of 0.1° is read into the program. The probe pattern is rotated about the z-axis in small increments that are multiples of the $\phi$ spacing by translating the elements of the data array for each iteration of the program. For the first iteration the rotation is zero. This probe rotation, and the evaluation of the transmission equation for each rotated probe pattern, produces the polarization pattern by producing a probe output for each rotation increment. Interpolation is used on each of the probe patterns to calculate $\theta$ and $\phi$ vector components on a grid that is equally spaced in $\frac{k_x}{k}$ and $\frac{k_y}{k}$ with Nx x Ny points over the span from -1 to +1 and is identical to the grid that was used for the test antenna far field pattern. The AZ and EL vector components are then calculated from the $\theta$ and $\phi$ vector components. Since the receiving plane wave spectrum $\vec{s}_{02}'(\vec{K},\chi)$ is identical to the far electric field pattern, the probe patterns for each rotation angle required for the transmission equation have now been produced.

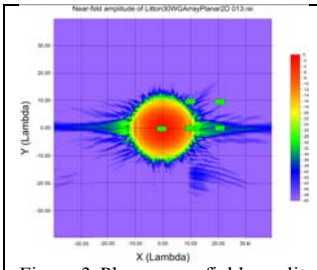


Figure 3-Planar near-field amplitude for the AUT used in the simulation showing the near-field x,y points where simulations will be produced.

Using the plot of the planar near-field amplitude of the AUT, shown in Figure 3 as a guide, a point in the near-field is selected for the simulation of a polarization measurement and its x, y, and z coordinates read into the simulation program. The AUT was a 24λ slotted waveguide array operating at 9.375 GHz. For the first example described in the following section, the point x=20λ, y=0, z=40λ denoted by one of the red rectangles was selected. The far electric field pattern for the antenna under test is then read into the program with the same number of points, span and spacing as the probe pattern just created. This pattern is already on a k-space grid using the AZ and EL vector components and so no interpolation or vector transformation is required. However the transmitting plane wave spectrum is not the same as the far electric field pattern and so the electric field pattern is divided by $\cos(\theta)$ to produce $\vec{t}_{10}(\vec{K})$ . The dot product of the AUT transmitting and probe receiving spectra, which is referred to as the coupling product, for each rotation angle is calculated at each point in the grid, the exponential factors involving the specified x, y, and z positions and the components of the propagation vector are also calculated for each point and multiplied by the spectral product as required in equation 3 to produce the convolution product. The convolution product is then summed over all Nx x Ny points of the k-space grid to produce the probe received signal for the specified probe position as a function of the rotation angle $\chi$ and this polarization data is saved for comparison to the polarization data that will be produced using the first-order probe data. Figures 4-12 illustrate the steps in the simulation. Figures 4 and 5 show the amplitudes for the AZ and EL components of the higher-order probe pattern for $\chi$ =0 and Figures 6 and 7 show the same data for $\chi$ = 90º. The change in the cross component patterns from EL to AZ component is evidence of the 90º rotation of the probe pattern. Figures 8 and 9 show the AZ and EL component amplitude patterns for the AUT. Figures 10 and 11 show the amplitude plots of the convolution product for $\chi$ = 0º and 90º respectively. Figure 11 is the dot product of Figures 4 and 5 with Figures 8 and 9 while Figure 11 is the dot product of Figures 6 and 7 with Figures 8 and 9. Figure 12 is the final output polarization curve for the higher-order probe.

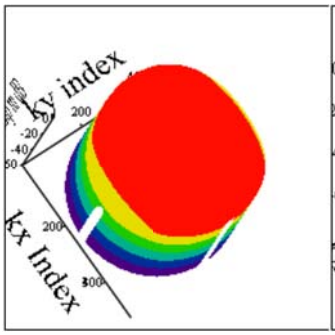


Figure 4- OEWG AZ component amplitude for 0 degrees χ rotation.

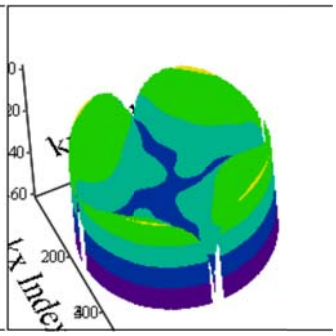

Figure 5- OEWG EL component amplitude for 0 degrees χ rotation

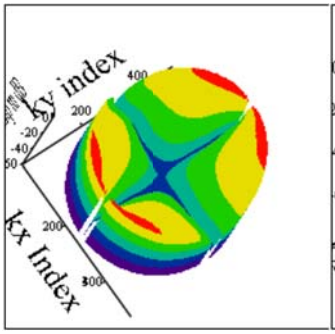


Figure 6- OEWG AZ component amplitude for 90 degrees χ rotation.

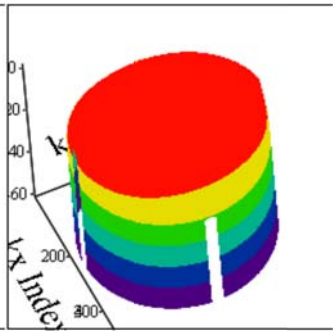

Figure7-OEWG EL component amplitude for 90 degrees χ rotation.

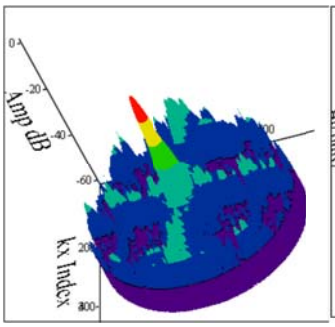


Figure 8- AUT AZ component plane wave transmitting spectrum.

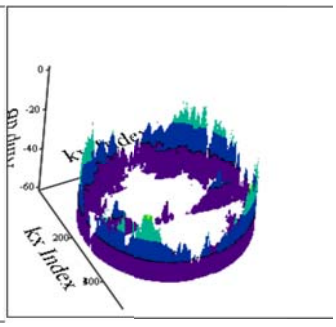

Figure 9-AUT EL component plane wave transmitting spectrum.

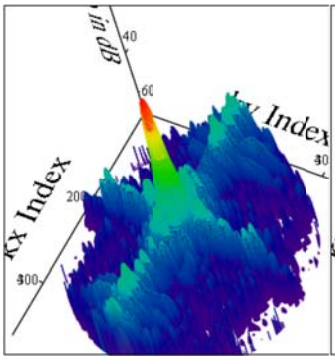


Figure 10- Convolution product amplitude for the higher-order probe at 0 degrees rotation angle.

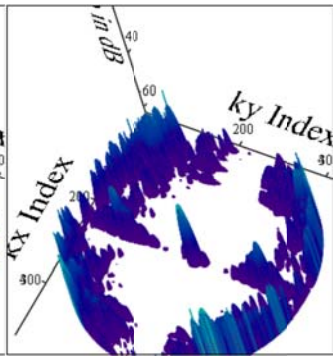


Figure 1-Convolution product amplitude for the higher-order probe at 90 degrees rotation angle.

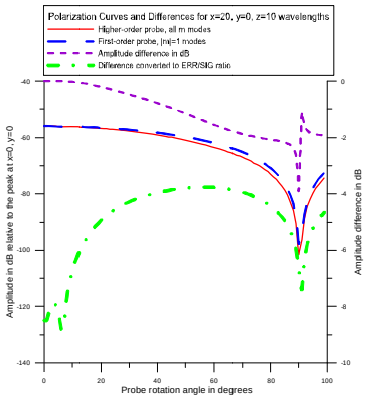


Figure 2-Sample polarization curves for the two probes and their differences for x = 20, y = 0, z = 10 wavelengths.

When the polarization curve for the higher-order probe has been produced and saved, the probe pattern for the first-order probe which has only the spherical modes for m=±1 is read into the program and data and graphics similar to Figures 5-12 are produced. The general character of graphical outputs for the first-order probe are very similar to those shown in Figures 5-11 and will not be shown here. A sensitive and quantitative measure of the difference between the two probes is obtained by comparing the polarization curves produced by the two probes as illustrated in Figure 12.

When the simulation program was fully developed and producing output curves like figure 12, a number of tests were run to verify the accuracy of the concept and the programs. Two separate simulation programs were actually developed and tested. Both authors produced programs using different software but the same input data, the same concepts and equations and the results of the two programs were the same. One program was used to calculate a near-field hologram by using a single probe rotation angle and calculating the probe output for a complete X-Y grid. The results agreed with the hologram produced by the NSI2000 software. Different resolutions were used for the initial probe patterns that were calculated using θ,φ coordinates. Angular increments as large as 1° for both angles were used with very little change in the output. All of the final results used 0.2° spacing in θ and 0.1° spacing in φ. For a few selected X-Y positions, the program was run for increasing Z distance to verify that the difference between the two probes polarization curves decreased with distance showing that the higher-order probe performed like a first-order probe for large separation distances. The on-axis amplitude and phase were also calculated for a single probe rotation angle to verify that these quantities varied as expected. In performing these last two tests, it was found that the array sizes for the AUT and probe that were used in calculating the planar transmission equation needed to be at least 1024 x 1024 to give correct results at Z distances of 80λ or larger. Since the primary interest was for small Z distances, this was not a limitation on the reliability of the results, and when large Z distances were used, the array sizes were increased as necessary.

Tests were also performed to demonstrate that the far-out side lobes of the AUT plane wave transmitting spectrum were not dominating the calculation of the polarization curves. The far-out side lobes derived from the planar near-field data are not reliable due to truncation of the near-field data, and for an actual antenna may be much lower than represented in the AUT far-field pattern. When the spectrum is calculated by dividing by the cos(θ) these lobes are significantly increased at the far-out angles. This can be seen in the high amplitude rings at the circular boundary of the plot in figures 9 and 11. If these lobes were dominating the calculation of the polarization curves, it could lead to erroneous results. To test this possibility, the polarization curves for some probe positions were recalculated after applying a filter to the plane wave transmitting specta. In these tests, the spectrum amplitudes beyond the filter limit were set to zero before the calculation of the coupling product. Filter limits of 90º, 80° and 40° were used and these filters did cause some change in the details of the polarization curves and the difference curves. However the general shape of the curves and especially the level of the difference curves showed only minor changes. This confirmed that since the same spectrum is used for both probes and as a result of the rapid phase change produced by the exponent in equation 3 near the boundary of the spectrum, these far-out lobes were not dominating the convolution product and leading to erroneous conclusions.

### 3.0 Results Summary

A large number of simulations were run for the slotted waveguide array antenna and for a standard gain horn at different X, Y and Z positions relative to the center of the antenna. To draw general conclusions from these results, a large amount of data needs to be condensed into a manageable format. The difference curves in figure 12 contain the important information about the errors that could result in a spherical near-field measurement by using the higher-order probe and then processing the data with software assuming that it had been measured with a first-order probe. The details of the polarization curves are not important and the amplitude difference in dB may have large spikes, but they are generally at low amplitudes. The first step in condensing the data is to focus on the ERR/SIG difference curves and a set of these for different probe positions is shown in Figure 13.

The difference curve for a given probe position is associated with a single point in the spherical near-field measurement array and is used to estimate the error at that single measurement point. The detailed shape of the difference curve is not important. The overall level of the curve relative to the near field peak amplitude is a good measure of the probable error. And so to include the full range of the difference curve in the estimated error, the RMS value of the ERR/SIG difference between the polarization amplitude curves as measured by the first order and higher-order probes was calculated for each test antenna and probe position and this RMS value is used as a predictor of the probable error in the spherical near-field measurement at that particular point. From tables or graphs of the RMS value for a number of points in the near-field, conclusions can then be drawn about the overall measurement and calculation uncertainty. The results for the slotted waveguide array are summarized in Table 1.

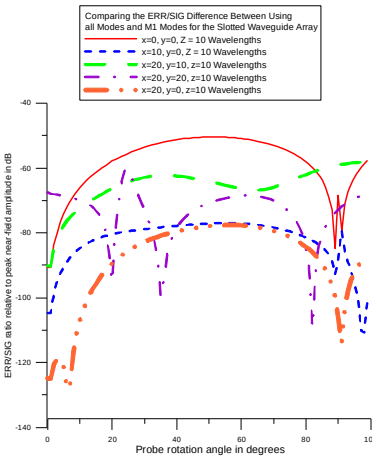

Figure 3-ERR/SIG curves for the slotted waveguide array at different x,y positions and z = 10 wavelength

Table 1-Summary of results for the slotted waveguide array as the AUT.

| | PROBE POSITION IN WAVELENGTHS | | | | | |
|---|---|---|---|---|---|---|
| AUT | X | Y | Z | FF PAT DIM | FILTER DEG | RMS DIFF (DB) |
| Array | 0 | 0 | 10 | 512 | 90 | -54 |
| Array | 10 | 0 | 10 | 512 | 90 | -80 |
| Array | 20 | 0 | 10 | 512 | 90 | -82 |
| Array | 20 | 10 | 10 | 512 | 90 | -63 |
| Array | 20 | 20 | 10 | 512 | 90 | -70 |
| Array | 0 | 0 | 20 | 512 | 80 | -68 |
| Array | 0 | 0 | 20 | 1024 | 80 | -68 |
| Array | 0 | 0 | 40 | 1024 | 80 | -79 |
| Array | 10 | 0 | 40 | 1024 | 80 | -55 |
| Array | 20 | 0 | 40 | 512 | 80 | -62 |
| Array | 20 | 0 | 40 | 512 | 89 | -62 |
| Array | 0 | 0 | 80 | 512 | 80 | -79 |
| Array | 0 | 0 | 100 | 512 | 80 | -71 |
| Array | 10 | 0 | 100 | 512 | 80 | -70 |
| Array | 0 | 0 | 200 | 512 | 80 | -65 |
| Array | 0 | 0 | 200 | 1024 | 80 | -82 |
| Array | 10 | 0 | 200 | 512 | 80 | -75 |

All of the comparisons between the two probes have focused on the amplitude differences and phase differences have not been reported here. Phase

differences in measured near-field data are very important and can lead to large differences in far-field patterns if the differences are large and have certain undesirable variation over the measurement surface. Phase difference curves were produced for all of the simulations and examined and it was found that typically the phase differences were close to 0º or 180º. There were some regions of larger differences similar to the amplitude spikes near-the nulls in the polarization curves. The observed phase differences should not change the conclusions based on the RMS amplitude differences.

In addition to the results using the slotted array as the AUT, simulations were also produced for an X-band standard gain horn (SGH) operating at the same frequency as the array. The results for the SGH are summarized in Table 2.

Table 2-Summary of the results for the SGH.

| | PROBE POSITION IN WAVELENGTHS | | | | | |
|---|---|---|---|---|---|---|
| AUT | X | Y | Z | FF PAT DIM | FILTER DEG | RMS DIFF (DB) |
| SGH | 0 | 0 | 10 | 256 | 90 | -60 |
| SGH | 0 | 0 | 20 | 512 | 80 | -72 |
| SGH | 0 | 0 | 40 | 512 | 80 | -69 |
| SGH | 0 | 6 | 10 | 512 | 80 | -48 |
| SGH | 6 | 0 | 10 | 512 | 80 | -53 |
| SGH | 0 | 10 | 20 | 256 | 80 | -63 |
| SGH | 0 | 6 | 20 | 256 | 90 | -73 |
| SGH | 0 | 10 | 20 | 256 | 90 | -62 |

## 4.0 Conclusions

For both antennas and for all the near-field points used in the simulation the general characters of the results were the same. The polarization patterns for both the first-order and higher-order probes were very similar but there were measurable differences indicating that the probes do produce different polarization patterns and would produce different far-field results if the standard spherical software was used. The RMS amplitude differences were all near or below -50 dB relative to the peak of the near-field amplitude and a majority were in the -60 to -80 dB range. These levels are significantly below typical error levels for other sources such as scattering, alignment, multiple reflections and leakage. The RMS levels were generally higher when the probe was at a low amplitude location outside the aperture region of the AUT and these near-field regions have less of an effect on the far-field patterns. Some of the probe positions were near the minimum sphere radius and a few were actually inside of the minimum sphere. When all of these facts are taken into consideration it is very unlikely that the errors caused by using an OEWG probe for near-field measurements in typical measurements could be distinguished from other larger error sources in an actual measurement. The effect of using an OEWG probe in a typical measurement is probably at the noise level of most measurements. This is true even when the measurement radius is close to the minimum sphere.

Further simulations could be done to apply error signals at the levels observed here to measured data using different functional forms for the errors as a function of position or measured signal level to quantify their effect on far-field parameters. The effect of phase differences in the polarization curves should also be analyzed further.

This simulation technique could also be used to determine the effect of using other probes that have higher levels for the higher order μ modes.

### 5.0 References


(1) Wacker, P.F. (1974), "Near-field antenna measurements using a spherical scan: Efficient data reduction with probe correction", *Conf. on Precision Electromagnetic Measurements*, IEE Conf. Publ. No. 113, pp. 286-288, London, UK.

(2) T. A. Laitinen, S. Pivnenko, and O. Breinbjerg, "Odd-order probe correction technique for spherical near-field antenna measurements," *Radio Sci.*, vol. 40, no. 5, 2005.

(3) T. A. Laitinen and O. Breinbjerg, "A first/third-order probe correction technique for spherical near-field antenna measurements using threeprobe orientations," *IEEE Trans. Antennas Propag.*, vol. 56, pp. 1259–1268, May 2008.

(4) T. Laitinen, J. M. Nielsen, S. Pivnenko, and O. Breinbjerg, "On the application range of general high-order probe correction technique in spherical near-field antenna measurements," presented at the 2nd Eur. Conf. on Antennas and Propagation (EuCAP'07), Edinburgh, U.K., Nov. 2007.

(5) T. A. Laitinen, S. Pivnenko, and O. Breinbjerg," Theory and Practice of the FFT/Matrix Inversion Technique for Probe-Corrected Spherical Near-Field Antenna Measurements With High-Order Probes," *IEEE Trans. Antennas Propag.*, vol. 58,, No. 8, pp. 2623–2631, August 2010.

(6) T. A. Laitinen, S. Pivnenko,"On the truncation of the azimuthal mode spectrum of high-order probes in probe-corrected spherical near-field antenna measurements" AMTA, Denver, November 2012.

(7) Kerns, D.M. (1976), "Plane-wave scattering.matrix theory of antennas and antenna-antenna interactions : formulation and applications", *J. Res. NBS*, Vol. 80B, No. 1, pp. 5-51.

(8) Jensen, F. (1975), "On the probe compensation for near-field measurements on a sphere", *Archiv für Elektronik und Übertragung-stechnik*, Vol. 29, No. 7/8, pp. 305-308.

(9) Hansen, J.E. (Ed.) (1988), *Spherical Near-Field Antenna Measurements*, Peter Peregrinus, Ltd., on behalf of IEE, London.

(10) A. C. Ludwig, "The definition of cross polarization," *IEEE Trans. AntennasPropag.*, vol. 21, pp. 116–119, Jan. 1973.

(11) Hindman, G, Newell, A.C., " Reflection Suppression in a large spherical near-field range", AMTA 27th Annual Meeting & Symposium, Newport, RI, Oct. 2005.

(12) Hindman, G, Newell, A.C., " Reflection Suppression To Improve Anechoic Chamber Performance", AMTA Europe 2006, Munch, Germany, Mar. 2006.